Generation of Human-like Motion for Humanoid Robots Based on Marker-based Motion Capture Data

Stefan Gärtner, Martin Do, Tamim Asfour, Rüdiger Dillmann
Karlsruhe Institute of Technology (KIT), Institute for Anthropomatics, Humanoids and Intelligence Laboratory, Karlsruhe, Germany

Christian Simonidis, Wolfgang Seemann
Karlsruhe Institute of Technology (KIT), Institute of Engineering Mechanics, Karlsruhe, Germany

Abstract

To increase acceptance for humanoids in everyday situations, it is essential that motions of humanoid robots become more human-like. A proper approach to achieve this requirement is introduced by adopting marker-based human motion capture. In order to efficiently re-use or analyze captured movements on various robots, an intermediate model, named Master Motor Map (MMM), is proposed which decouples representation of motion from its execution on a real robot. Moreover, we present a constrained nonlinear optimization to adapt pre-captured motions to our robot Armar-III preserving necessary motion characteristics and preventing the robot from approaching specific limitations.

1 Introduction

Since humanoid robots increasingly become part of our everyday lives, they will serve as caretakers for the elderly and handicapped people as well as assistants in various situations. For this purpose, it is essential that motions on such a robot appear more human-like and less artificial. However, for this to happen, programming and control of motions and skills on such a robot must become simpler and more intuitive.

Adaption of pre-recorded motions from human observation for controlling a robot constitutes a promising approach. Regarding this challenge, motions must be mapped to a given robot while preserving important human-like characteristics and, on the contrary, they must satisfy task-specific requirements. To achieve this goal, we focused on an approach applying constrained large-scale nonlinear optimization.

There exist numerous human motion capture systems that produce output in terms of different models that are stored in different formats making it more difficult to exchange modules in an overall infrastructure for humanoid robots. To overcome this problem, the Master Motor Map (MMM), firstly introduced in [1], represents an appropriate framework to decouple motion capture data from further post-processing tasks. The essential part of the MMM framework is a unified model that supports mapping between different kinematics, independently and uniformly. Since the effort is very high to create a model for each subject individually, a unified model that can be scaled in terms of body weight and height is also useful. To use this model, for example, in terms of determining forward and inverse dynamics, dynamic segment properties such as mass distribution are required. Furthermore, common benchmarks as well as evaluation methods in humanoid robotics become only feasible when a common representation for human motion is shared.

To demonstrate the applicability of our approach, we transfer various pre-captured motions to our humanoid robot ARMAR-III being developed for applications in human-centered environments [2]. The robot as shown in **figure 1** is equipped with manipulative, perceptive, and communicative skills necessary for real-time interaction with the environment and humans.

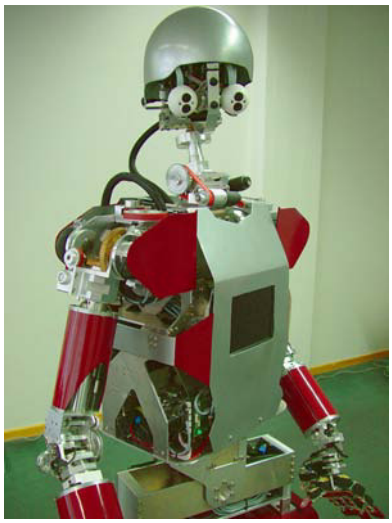

Figure 1: The humanoid robot ARMAR-III.

In section 2, we list related work from both, biomechanics and robotics, to give an overview of biomechanic modeling

ISBN 978-3-8007-3273-9

of humans as well as transferring and editing pre-captured motions. The extension of the MMM model is explained in section 3. The actual method to map pre-captured motions to the proposed anthropometric model is presented in section 4. Experimental results are shown in section 5.

2 Related Research

Generation of human-like motions has become a meaningful technique for biomechanics and robotics. Although the emphasis in both communities differs, an increasing number of methods that rely on motion capture data is used by both. From a biomechanic perspective, human motion capture data are utilized for example to extract fundamental principles of motion [3] or to improve meaningful parameters of biomechanic models [4]. On the contrary, the key research areas in robotics are motion re-targeting, execution on a real robot and generalization.

Several approaches [5, 6, 7, 8] have been proposed in previous research to compute feasible joint angle trajectories in order to control upper body motions for a humanoid robot in free-space applying non-linear optimization. Furthermore, in [9], a novel approach is proposed to map from three-dimensional marker position data recorded by optical motion capture systems to joint angle trajectories for a skeleton with fixed limb lengths. According to the optimization approach, another objective function that considers end-effector positions directly to determine joint angle trajectories is introduced in [10].

Most of the mentioned approaches directly adapt motion to the kinematic structure of the used humanoid robot without considering intermediate models at all. Thus, further application of the motion is restricted to the robot used in the first place. For facilitating human motion data, researchers have focused on storing motions in proper repositories. On that account, sufficient intermediate models are required that are complex enough to meet most requirements from research and simple enough to be practicable.

Over the last decades, a lot of attempts have been made to develop sufficient dynamic models for simulating and analyzing complex motions of the human. Various biomechanic models are thoroughly reviewed in [11]. The morphology of an anthropomorphic mathematical-geometrical model of the segmented human body defines the number of mechanical degrees of freedom (DoF) as well as the shapes and inertial properties of the individual segment required to calculate forward and inverse dynamics. In numerous publications [12, 13, 14, 15, 16, 17, 18] body segment properties are reported differing in gender and ethnic group of the subjects as well as in measurement methods that were applied to obtain the properties. Many of the predictive equations generated from data are based on regression methods or are equations based on geometric considerations. Linear regressions such as scaling equations, based on total body mass and segment length, are commonly used because of their expediency.

3 Model

The essential part of the MMM framework is based on a three-dimensional whole-body, kinematic model enriched with proper body segment properties (BSP), such as mass distribution, segment length, moment of inertia, etc., in order to compute gross body dynamics. The strategy with respect to the kinematic model is to define the maximum number of DoF that might be used by any visualization, recognition or reproduction module used on a humanoid robot. The kinematic model of the MMM framework including DoF and the Euler angle conventions is shown in **table 1**.

Joint	**DoF**	**Euler Angles**
Root	6	$R_{X'Z'Y'}(\alpha,\beta,\gamma)$
Pelvis	3	$R_{X'Z'Y'}(\alpha,\beta,\gamma)$
Torso	3	$R_{X'Z'Y'}(\alpha,\beta,\gamma)$
Neck	3	$R_{X'Z'Y'}(\alpha,\beta,\gamma)$
Skullbase	3	$R_{X'Z'Y'}(\alpha,\beta,\gamma)$
Hip R/L	3 + 3	$R_{X'Z'Y'}(\alpha,\beta,\gamma)$
Knee R/L	1 + 1	$R_{X'Z'Y'}(\alpha,0,0)$
Ankle R/L	3 + 3	$R_{X'Z'Y'}(\alpha,\beta,\gamma)$
Toe R/L	1 + 1	$R_{X'Z'Y'}(0,\beta,0)$
Sternoclavicular R/L	3 + 3	$R_{X'Z'Y'}(\alpha,\beta,\gamma)$
Shoulder R/L	3 + 3	$R_{X'Z'Y'}(\alpha,\beta,\gamma)$
Elbow R/L	2 + 2	$R_{X'Z'Y'}(\alpha,\beta,0)$
Wrist R/L	2 + 2	$R_{X'Z'Y'}(\alpha,0,\gamma)$
Total	**54**	

Table 1: Number of DoF and Euler angle conventions for the joints of the MMM model.

The process of defining anthropomorphic properties of the individual segments is guided by choices and scalings in anthropometric tables and linear regression equations. For this purpose, the linear equations from [16] are applied to the model as they represent the most complete and practical series of predictive equations for college-aged Caucasian adults providing all frontal, sagittal, and horizontal moments of inertia. The body segment properties are adjusted with respect to the kinematics of the MMM and listed in **table 2**. Users are cautioned not to apply the proposed model outside the population from which they were derived. However, little options are available when the research subject under study is not represented in the literature.

Since the effort is very high to create an anthropomorphic model for each subject individually, the proposed unified MMM model is used instead which can be scaled with respect to total body weight and length that are convenient and easy to use in practice. In the following, it is shown how these properties are used correctly to determine various dynamic properties of a segment e.g. the thigh. The

ISBN 978-3-8007-3273-9

moment of inertia tensor is computed by

$$I_{Thigh} = 0.14 \cdot M \cdot (0.288 \cdot L)^2 \cdot \begin{pmatrix} 0.25 & 0 & 0 \\ 0 & 0.114 & 0 \\ 0 & 0 & 0.25 \end{pmatrix}^2$$

where M is the total body weight and L is the total body height of the considered subject. The position of the center of mass in the local coordinate system of a segment is likewise determined by

$$r_{Thigh} = \begin{pmatrix} 0 \\ -0.33 \\ 0 \end{pmatrix} \cdot 0.288 \cdot L.$$

An anthropomorphic, voluminous model is useful in terms of motion synthesis, adaption, and analysis. To determine a sufficient voluminous model from the applied anthropometric data set, simple geometric primitives are employed that only have a few parameters to adjust. As an appropriate primitive, which also fits the human shape well, we decided to utilize cylinders. The radius r_i of the cylinder corresponding to segment i is determined by

$$r_i = \sqrt{\frac{M_i}{\rho_i \cdot L_i \cdot \Pi}},$$

where ρ_i is the density, M_i the mass, and L_i the length of the regarded segment.

4 Motion Generation

Our approach of adapting movements consists of two major constrained large-scale nonlinear optimizations covering different requirements as illustrated in **figure 2**. The first optimization transfers a pre-captured motion to the articulated MMM model which can be stored in a motion repository for further processing (section 4.1). To finally execute movements on the humanoid robot ARMAR-III, a transformation from MMM to ARMAR-III requires another constrained non-linear optimization (section 4.2) differing in terms of additional task-specific requirements.

4.1 Conversion to MMM

In our approach, we use motions represented by three-dimensional marker trajectories that can be captured with a sophisticated marker-based motion capture system such as Vicon. One difficult problem, specifically related to transferring marker-based motion data to an articulated model, is the non-trivial mapping of the three-dimensional marker positions to a motion defined by joint angles. For this purpose, constrained large-scale nonlinear optimization is applied frame by frame. As optimization method to minimize the objective function, sequential quadratic programming (SQP) [19] is used. SQP is one of the most popular and robust algorithms which has been proved highly effective for solving constrained optimization problems with smooth nonlinear functions.

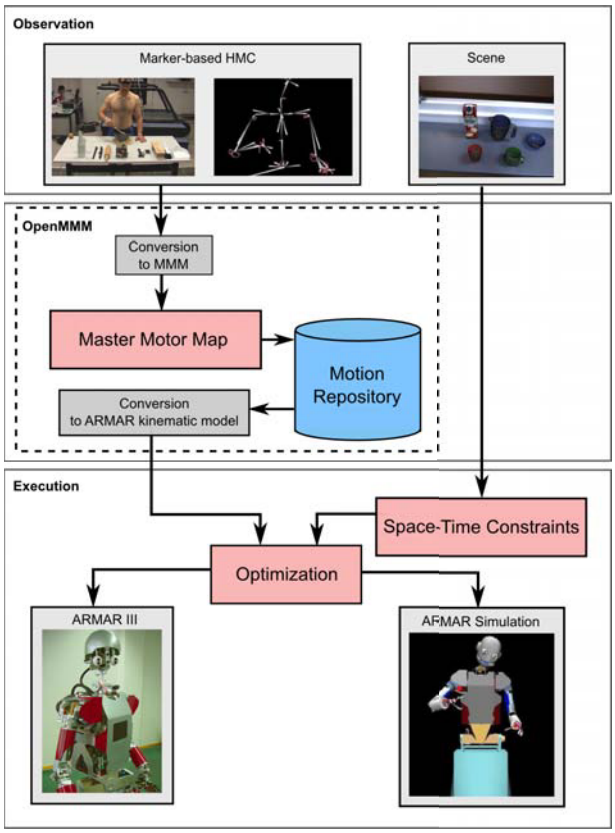

Figure 2: Overview of the proposed system.

4.1.1 Definition of an Objective Function and Constraints

The objective function should maintain desirable properties of the motion and should refuse undesirable artifacts which might appear unnatural. For this reason, a proper objective function contains components that preserve oscillations and the overall configuration as well as components that prevent the model from approaching specific limitations. In our approach, the objective function is therefore based on minimization of the sum of the squared distance between pre-captured and virtual markers expressed as:

$$F(\Theta_t) = \frac{1}{2} \Delta y(t, \Theta_t)^T \mathbf{W} \Delta y(t, \Theta_t) \qquad (1)$$

subject to

$$l \leq \begin{pmatrix} \Theta_t \\ f(\Theta_t) \\ A_L \Theta_t \end{pmatrix} \leq u,$$

where $\Delta y(t, \Theta_t)$ is denoted by

$$\Delta y(t, \Theta_t) = \widetilde{y}(\Theta_t) - y(t).$$

ISBN 978-3-8007-3273-9

Segment	Segment Length/ Total Body Height	Segment Weight/ Total Body Weight	Center of Mass/ Segment Length [x y z]			Radius of Gyration/ Segment Length [rxx, ryy, rzz]		
Hip	0.26	0.11	[0	4	0]	[38	36.5	34]
Spine	0.10	0.10	[4	46	0]	[32	26	28.6]
Chest	0.18	0.17	[0	46	0]	[35	28.5	31.3]
Neck	0.05	0.024	[0	20	0]	[31.6	22	31.6]
Head	0.13	0.07	[12	13	0]	[31	26	30]
Shoulder R/L	0.10	0.021	[0	0	-66]	[26	26	12]
Upper Arm R/L	0.16	0.027	[0	-57.3	0]	[26.8	15.7	28.4]
Lower Arm R/L	0.13	0.016	[0	-53.3	0]	[31	14	32]
Hand R/L	0.11	0.006	[0	-36	0]	[23.5	18	29]
Thigh R/L	0.25	0.14	[0	-33	0]	[25	11.4	25]
Shank R/L	0.23	0.04	[0	-44	0]	[25.4	10.5	26.4]
Foot R/L	0.15	0.013	[39	-6	0]	[12	19.5	21]

Table 2: Adjusted body segment properties for the MMM model. Segment masses are relative to body masses; segment lengths are relative to body heights. Both segment center of mass and radii of gyration are relative to the respective segment lengths.

Here, $\Theta_t = \{\Theta_1(t), \ldots, \Theta_N(t)\}$ are joint angles of the considered model; $\widetilde{y}$ are virtual markers that particularly correspond to pre-captured markers y; $\mathbf{W}$ is a pre-defined weighting matrix that can be used to indicate the importance of certain markers; $f(\star)$ is a smooth non-linear constraint and A_L a sparse matrix representing linear constraints. Upper and lower limits of the considered constraints are stored in u and l. Here, constraints are mainly associated with anatomic limitations of human extremities. Virtual markers are defined as fixed and pre-labeled points onto the surface of the voluminous anthropomorphic model which have to be set up in advance. Mathematically speaking, a virtual marker $\widetilde{y}_j$ is defined by

$$\widetilde{y}_j(\Theta_t) = [\prod_{i=0}^{N} A_i(\Theta_t)]\hat{y}_j = h_j(R(t), o(t), \Theta_t),$$

where A_i is a homogeneous transformation matrix determined by using Euler angles of the proposed MMM model, $\hat{y}_j$ is the local position of the considered virtual marker j, o is the position and rotation matrix R the orientation of the root. Furthermore, each virtual marker is defined by its bone position of the considered segment and a direction vector denoting a line which intersection point with the associated cylinder indicates the local virtual marker position $\hat{y}_j$. The used virtual marker set is illustrated in **figure 3**.
To avoid large differences in the model configuration at adjacent time steps, resulting in considerable jerks leading to shaky and unnatural-looking motions, caused by locally optimal solutions, markers of adjacent time steps are considered by adding a preview term to the objective function. For this, a function F_{t_k} is defined by

$$F_{t_k}(\Theta_t) = \frac{1}{2}\Delta y(t_k, \Theta_t)^T \mathbf{W} \Delta y(t_k, \Theta_t).$$

The objective function as denoted in equation 1 is then redefined using function F_{t_k} by

$$F(\Theta_t) = \sum_{i=0}^{T} \alpha_i F_{t+i}(\Theta_t).$$

Thus, succeeding markers have influence on the computation of the actual configuration which is decreasing with the distance to the actual frame explicitly modeled by α_i. The objective function without considering adjacent time steps is denoted accordingly as $F(\Theta_t) = F_t(\Theta_t)$.

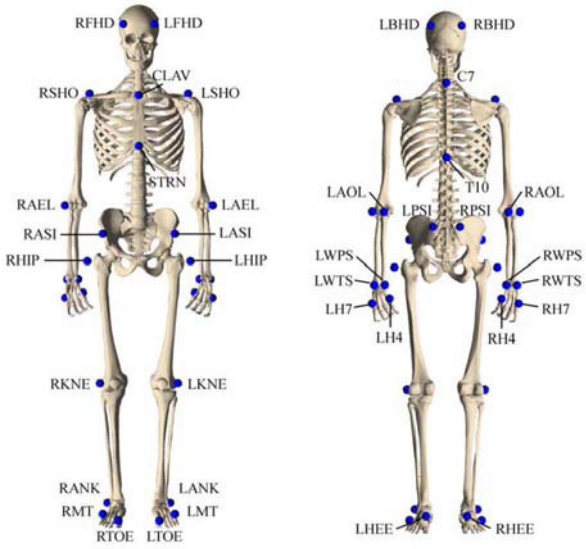

Figure 3: Applied marker set for capturing whole-body motions of a human.

ISBN 978-3-8007-3273-9

Since the actor's and the model's body shape are different due to simplification of design, a compensatory component must be added to the objective function. Furthermore, the term also accounts for misplaced markers and can be visualized as an elastic band between pre-captured and corresponding virtual markers whose springiness is decreasing over time. According to this, the mentioned aspect is integrated in the objective function, defined in equation 1, as follows

$$F(\Theta_t) = \frac{1}{2}(\Delta y(t, \Theta_t) - d(t))^T \mathbf{W}(\Delta y(t, \Theta_t) - d(t))$$

in which the function $d(t)$ is computed recursively by

$$d(t+1) = d(t) + \gamma^t \left\| \Delta y(t, \Theta_t) \right\|$$

at the beginning of time step $t+1$. The parameter γ models the stiffness and must be set up in advance. An initial value is given by

$$d(0) = 0.$$

As to preserve certain configurations of the pre-captured motion, additional constraints such as position, velocity, and acceleration of pre-defined reference points at particular time steps are used. A reference points is a point onto the surface of the considered model which has an accentuated importance. Following additional constraints cover the mentioned issue:

$$\begin{array}{rcccl} q(t) - \epsilon_{pos} & \leq & p(t) & \leq & q(t) + \epsilon_{pos} \\ \dot{q}(t) - \epsilon_{vel} & \leq & \dot{p}(t) & \leq & \dot{q}(t) + \epsilon_{vel} \\ \ddot{q}(t) - \epsilon_{acc} & \leq & \ddot{p}(t) & \leq & \ddot{q}(t) + \epsilon_{acc}. \end{array}$$

Function q is the desired and p the current trajectory of certain reference points. Therefore, function q can be determined by using either the pre-captured marker set or particular trajectory planning methods.

4.1.2 Determining an Initial Pose

In order to make raw marker data available for optimization, one has to determine the position, orientation, and scaling of the pre-captured marker set to transform markers into model space. In this research, local displacement and scaling of segments are permitted to preserve the natural appearance of the mapped motion. Thus, only one homogeneous transformation matrix for all markers must be determined initially by using the first frame of the pre-captured motion.
The mentioned problem can be solved sufficiently by applying the basic objective function as defined in equation 1. Here, the aforementioned pre-captured markers y are separately expressed as

$$y_j(t) = \mathbf{T}\bar{y}_j(t),$$

where $\bar{y}_j$ represents raw marker data of marker j and T the sought homogeneous matrix as mentioned before.

Assuming that no initial pose with the actor was agreed or addition knowledge about certain markers are available, a solution is quite difficult to find methodically. For this reason, a genetic algorithm is utilized in our approach.

4.1.3 Filtering the Transferred Motion

Since the proposed method considers each frame almost independently, slightly different alterations to each frame are determined according to local minima of the objective function. As a result, noise, contributed heavily to the high-frequency components is added to the motion. However, details of a motion that account for the natural look are also included in high-frequency components as represented in [20]. In order to suppress noise, pragmatic solutions, such as low-pass filtering, outweigh most other choices with respect to the design of an objective function. According to that, the Butterworth low-pass filter is applied in our approach which is introduced in [21].

4.2 Conversion to ARMAR kinematic model

Due to the differences in the kinematic structures of the MMM model and our humanoid platform ARMAR-III e.g. differing joints and limb measurements, in general, a one-to-one mapping does not lead to a goal-directed and human-like reproduction of a human movement. Therefore, in two stages, the joint angles, given in the MMM format, are optimized concerning the tool center point (TCP) position and the kinematic structure of the robot. First, a feasible solution is estimated, which serves as an initial solution for an optimization step in the second stage. Following this scheme, one obtains a human-like motion on the robot, while preserving its goal-directed characteristics.

4.2.1 Similarity Measure

One of the most crucial factors in the reproduction of human motion is the measure for rating the similarity between the imitated and the demonstrated movement. To achieve a trade-off between goal-directedness and human-likeness, both, the joint angle configuration $\Theta_t \in \mathbb{R}^n$ with n joints and key point correspondences, are combined in a similarity measure which is defined as follows:

$$S(\Theta_t) = 2 - \frac{\sum_{i=1}^{n} \left(\hat{\Theta}_i(t) - \Theta_i(t) \right)^2}{n\pi^2} - \frac{\sum_{i=1}^{3} \left(\hat{p}_k(t) - p_k(t) \right)^2}{3 \left(2 \cdot l_{arm} \right)^2} \tag{2}$$

with $\Theta_i(t), \hat{\Theta}_i(t) \in [0, \pi]$ and $p_k(t), \hat{p}_k(t) \in [-l_{arm}, l_{arm}]$, whereas l_{arm} describes the robots arm length. The reference joint angle configuration is denoted by $\hat{\Theta}_t \in \mathbb{R}^n$, while $\hat{p}_t \in \mathbb{R}^3$ stands for the desired TCP position. The current TCP position p_t can be determined by applying the forward kinematics of the robot to the joint angle configuration Θ_t.

ISBN 978-3-8007-3273-9

4.2.2 Estimation of an Initial Solution

To obtain a posture, which bears a high resemblance to the one of the human and at the same time meets all the mechanical constraints of the robot, the original joint angle configuration is optimized using Levenberg- Marquardt (LM) regarding the similarity measure as specified in equation 2. To avoid being trapped in local extrema, an initial estimation Θ^{init} is generated from the reference joint angle configuration $\hat{\Theta}_t$ by first projecting on the bound constraints:

$$\hat{\Theta}_i(t) = \begin{cases} C_{i_{min}} & \text{if } \hat{\Theta}_i(t) \leq C_{i_{min}} \\ \hat{\Theta}_i(t) & \text{if } C_{i_{min}} \leq \hat{\Theta}_i(t) \leq C_{i_{max}} \\ C_{i_{max}} & \text{if } \hat{\Theta}_i(t) \geq C_{i_{max}} \end{cases}$$

where $C_{i_{min}}$ and $C_{i_{max}}$ denote the lower and upper joint angle bounds of joint i. If the value of $\hat{\Theta}_i(t)$ exceeds the given bounds, the joint i is fixed at the closest of the two boundaries. In addition to constraining, each non-fixed joint angle of Θ^{init} is altered by means of a vector $\delta_t \in \mathbb{R}^n$ with $\delta_i(t) = \hat{\Theta}_i(t) - \hat{\Theta}_i(t-1)$. Thus, δ_t describes the changes between two consecutive frames. As a result, a candidate initial estimation Θ^j can be described as:

$$\Theta_i^j = \hat{\Theta}_i(t) + \alpha_i \beta_i$$

with

$$\alpha_i = \begin{cases} 1 & \text{if } C_{i_{min}} \leq \hat{\Theta}_i(t) \leq C_{i_{max}} \\ 0 & \text{else} \end{cases}$$

$$\beta_i \in \{-\delta_i(t), 0, \delta_i(t)\}$$

Given n joints to control, in the worst case $M = 3^n$ candidates need to be calculated and evaluated. The best initial estimation satisfies the following equation:

$$\Theta^{init} = \underset{j=1,\ldots,M}{\arg\max}\, S(\Theta^j) - \|\hat{\Theta}_t - \Theta^j\|$$

Finding the best initial estimation causes some overhead regarding processing time, but it is necessary to ensure that the following optimization procedure will provide an optimal solution.

4.2.3 Optimization Problem

Using the LM algorithm, the reference joint angle configuration $\hat{\Theta}_t$ concerning the similarity measure is optimized. The corresponding optimization problem can be written in the following form:

$$\begin{aligned} & \min S'(\Theta_t) = 2 - S(\Theta_t) \\ \text{subject to} \quad & C_{i_{min}} \leq \hat{\Theta}_i(t) \leq C_{i_{max}} \end{aligned}$$

which is equivalent to the maximization of equation 2. More practical details on the algorithm can be found in [10].

5 Experiments

In this section, experimental results of the proposed system with a marker-based human motion capture system are shown. The hardware setup which was used to capture the human motion consists of eight Vicon cameras. Since using a marker-based approach allows to capture a large set of degrees of freedom, the number of active joint angle adds up to 24 DoF (ten for each arm, three DoF for the head and one DoF for the hip rotation). The first experiment focused on the reproduction of reaching movements on ARMAR-III in a human-centered environment by constraining the position of the TCP to a specific location. In the second experiment, an object lifting movement is analyzed in terms of dynamics by using the MMM model to obtain a executable motion on the ARMAR robot.

5.1 Experiment 1: Adapting the TCP Position to Satisfy Reaching Requirements

In this experiment, a pre-captured reaching motion is optimized in terms of different TCP positions. The motion is reproduced on ARMAR-III in simulation. The original target position of the TCP in the global coordinate system is located at $(-542, -91, 23)$ whereas the units are represented in mm. For different TCP target positions $T1 = (-300, 300, 100)$, $T2 = (-400, 300, 100)$, and $T3 = (-400, 300, 100)$ motions are generated based on the original one. In T4, the TCP position is kept unchanged for comparison. Changing the desired TCP position leads to an adaption of the joint angles in order to reach a position close to the target. The averaged joint angle errors over all joints for $T1$, $T2$, and $T3$ are illustrated in **figure 4** in radians.

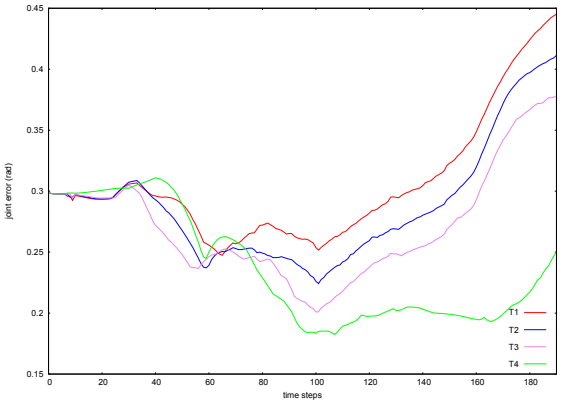

Figure 4: Joint error of the adapted motions T1 to T4.

The error rises for desired positions, which are farther away from the original TCP position. Nevertheless, due to the optimization procedure, the joint angle modifications could be minimized, whereas the resulting TCP position could not be aligned exactly with the desired target, but to a close position. The corresponding TCP errors for $T1$,

ISBN 978-3-8007-3273-9

$T2$, and $T3$ are depicted in **figure 5**. This behaviour states a tradeoff between exact reaching via inverse kinematics and regarding the joint angle error a lossless one-to-one mapping between both embodiments.

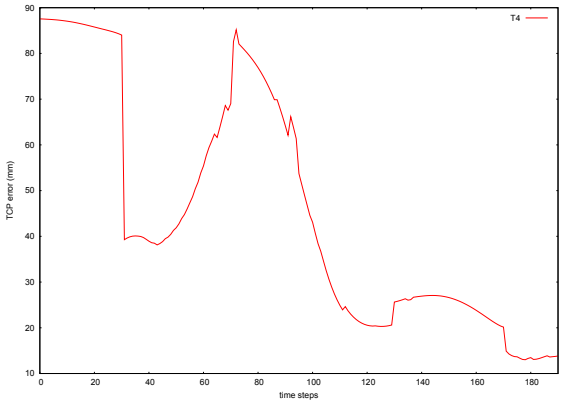

Figure 5: Error between the original TCP position in MMM and the TCP position scaled and transformed to the ARMAR hip coordinate system.

5.2 Experiment 2: Analyzing and Constraining an Object Lifting Motion

In this experiment, an object lifting motion is transferred to the proposed MMM model. The pre-captured motion has an original length of about 2 seconds and the object has a weight of 0.5 kg. In **figure 6**, torque trajectories for each DoF of the left arm are illustrated which have been obtained by applying Newton-Euler.

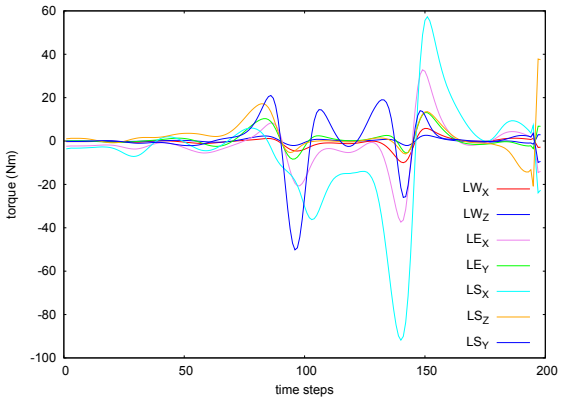

Figure 6: Joint torque trajectories of the pre-captured object lifting motion.

As seen in this figure, the shoulder torque reaches a peak of about -90 Nm which is too large for execution on the humanoid robot ARMAR-III. In order to properly reduce the shoulder torque while preserving the human-like appearance, the motion must be slowed down properly. Applying constrained optimization, we attained a motion with reduced shoulder torque that is 5.25 times slower than the original motion. In **figure 7**, the joint torque trajectories are presented.

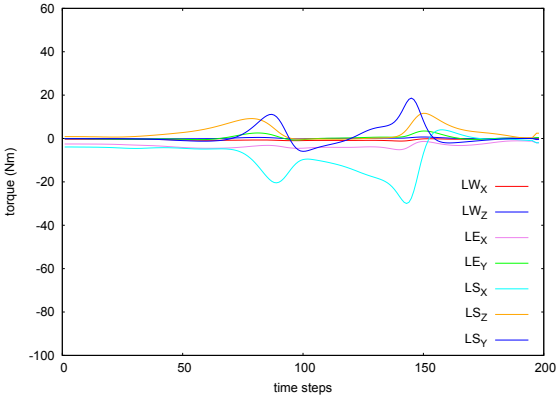

Figure 7: Joint torque trajectories of the object lifting motion that is slowed down by a factor of 5.25.

The absolute maximum torque is set up to 30 Nm according to the mechanical limitations of the shoulder joint. The determined motion can be transferred to the robot as demonstrated in the first experiment.

6 Conclusion

In this work, we have investigated the problem of transferring a pre-captured human motion to the humanoid robot ARMAR-III by applying an intermediate whole-body model and a constrained large scale non-linear optimization. In order to determine gross dynamic aspects of human motion, the mentioned reference model have been enriched with body segment properties taken from previous studies in biomechanics. Moreover, experiments have been provided to demonstrate how pre-captured motions must be adapted satisfying pre-defined requirements. Therefore, we have focused on reproducing positional changes on the surface of the robot rather than changes in joint angle space, so that human-like characteristics of the pre-captured motion are maintained.
In the near future, we will focus on analyzing numerous pre-captured human motion data with the proposed system in order to develop more sophisticated motion pattern generators for various applications in robotics.

7 Acknowledgment

The work described in this paper was partially conducted within the EU GRASP (FP7-215821) funded by the European Commission and the German Humanoid Research project SFB588 funded by the German Research Foundation (DFG: Deutsche Forschungsgemeinschaft).

ISBN 978-3-8007-3273-9

References

[1] P. Azad, T. Asfour, and R. Dillmann, "Toward an unified representation for imitation of human motion on humanoids," *Robotics and Automation, 2007 IEEE International Conference on*, pp. 2558 – 2563, 2007.

[2] T. Asfour, K. Regenstein, P. Azad, J. Schroeder, A. Bierbaum, N. Vahrenkamp, and R. Dillmann, "Armar-iii: An integrated humanoid platform for sensory-motor control," *IEEE-RAS International Conference on Humanoid Robots, Proceedings*, 2006.

[3] C. Simonidis and W. Seemann, "Improving marker based inverse kinematics solutions for underdetermined spinal models," in *Computational Kinematics, Proceedings of the 5th International Workshop on Computational Kinematics*, A. Kecskemethy and A. Mueller, Eds. Heidelberg: Springer, 2009.

[4] C. Simonidis, T. Stein, F. Bauer, A. Fischer, H. Schwameder, and W. Seemann, "Determining principles of human motion by combining motion analysis and motion synthesis," in *Proceedings of the IEEE-RAS International Conference on Humanoid Robots*, Paris (France), 2009.

[5] T.-W. Lu and J. O'Connor, "Bone position estimation from skin marker co-ordinates using global optimisation with joint constraints," *Journal of Biomechanics*, vol. 32, pp. 129–134, 1999.

[6] M. Riley, A. Ude, and C. Atkeson, "Methods for motion generation and interaction with a humanoid robot: Case studies of dancing and catching," *AAAI and CMU Workshop on Interactive Robotics and Entertainment 2000*, 2000.

[7] N. Pollard, J. Hodgins, M. Riley, and C. Atkeson, "Adapting human motion for the control of a humanoid robot," *Proceedings of the IEEE International Conference on Robotics and Automation (ICRA 02)*, 2002.

[8] A. Safonova, N. S. Pollard, and J. K. Hodgins, "Optimizing human motion for the control of a humanoid robot," *Adaptive Motion of Animals and Machines (AMAM2003), 2nd International Symposium on*, 2003.

[9] V. B. Zordan and N. C. Van Der Horst, "Mapping optical motion capture data to skeletal motion using a physical model," *Proceedings of the 2003 ACM SIGGRAPH/Eurographics symposium on Computer animation*, pp. 245 – 250, 2003.

[10] M. Do, P. Azad, T. Asfour, and R. Dillmann, "Imitation of human motion on a humanoid robot using nonlinear optimization," in *International Conference on Humanoid Robots (Humanoids 2008)*, 2008.

[11] A. I. King, "A review of biomechanical models," *Journal of biomechanical engineering*, vol. 106, pp. 97–104, 1984.

[12] J. T. Barter, "Estirnation of the mass of body segments," Wright Air Development Center, Wright-Patterson Air Force Base, Ohio, WADC Technical Report 57-260, April 1957.

[13] R. Chandler, C. Clauser, J. Mcconville, H. Renolds, and J. Young, "Investigation of the inertial properties of the human body." National Technical Information Service, Virginia, Tech. Rep., 1975.

[14] H. Hatze, "A mathematical model for the computational determination of parameter values of anthropomorphic segments," *Journal of biomechanical engineering*, vol. 13, pp. 833–843, 1980.

[15] V. Zatsiorsky, V. Seluyanov, and L. G. Chugunova, "Methods of determining mass-inertial characteristics of human body segments," *Contemporary Problems of Biomechanics*, pp. 272–291, 1990.

[16] P. de Leva, "Adjustments to zatsiorsky-seluyanov's segment inertia parameters," *Journal of Biomechanics*, vol. 29, no. 9, pp. 1223–1230, 1996.

[17] D. A. Winter, *Biomechanics and motor control of human movement*, 3rd ed. Hoboken, NJ: Wiley, 2005.

[18] R. Dumas, L. Cheze, and J.-P. Verriest, "Adjustments to mcconville et al. and young et al. body segment inertial parameters," *Journal of Biomechanics*, vol. 40, pp. 543–553, 2007.

[19] P. E. Gill, W. Murray, and M. A. Saunders, "Snopt - an sqp algorithm for large-scale constrained optimization," *SIAM Journal on Optimization*, vol. 4, pp. 99–131, 2005.

[20] K. Pullen and C. Bregler, "Motion capture assisted animation: Texturing and synthesis," *SIGGRAPH 2002*, vol. 21, pp. 501–508, 2002.

[21] R. Genesio, A. Laurentini, V. Mauro, and A. Meo, *Butterworth and Chebyshev Digital Filters: Tables for their design*. Elsevier Scientific Publishing Company, Amsterdam, 1973.

ISBN 978-3-8007-3273-9